Title

Production of cytoplasmic type citrus leprosis virus-like particles by plant molecular farming

Authors

Ortega-Rivera, Oscar A

Beiss, Veronique

Osota, Elizabeth O

et al.

Publication Date

2023

DOI

10.1016/j.virol.2022.11.004

Peer reviewed

HHS Public Access

Author manuscript

Virology. Author manuscript; available in PMC 2024 January 01.

Published in final edited form as:

Virology. 2023 January ; 578: 7–12. doi:10.1016/j.virol.2022.11.004.

Production of cytoplasmic type citrus leprosis virus-like particles by plant molecular farming

Oscar A. Ortega-Rivera[1,2], **Veronique Beiss**[1,2], **Elizabeth O. Osota**[1,2], **Soo Khim Chan**[1,2], **Sweta Karan**[1,2], **Nicole F. Steinmetz**[1,2,3,4,5,6,*]

[1]Department of NanoEngineering, University of California-San Diego, La Jolla CA 92039, USA

[2]Center for Nano-ImmunoEngineering, University of California-San Diego, La Jolla CA 92039, USA

[3]Institute for Materials Discovery and Design, University of California-San Diego, La Jolla CA 92039, USA

[4]Department of Bioengineering, University of California-San Diego, La Jolla CA 92039, USA

[5]Department of Radiology, University of California-San Diego, La Jolla CA 92039, USA

[6]Moores Cancer Center, University of California-San Diego, La Jolla CA 92039, USA

Abstract

Many plant virus-like particles (VLPs) utilized in nanotechnology are 30-nm icosahedrons. To expand the VLP platforms, we produced VLPs of Cytoplasmic type citrus leprosis virus (CiLV-C) in *Nicotiana benthamiana*. We were interested in CiLV-C because of its unique bacilliform shape (60–70 nm × 110–120 nm). The CiLV-C capsid protein (p29) gene was transferred to the pTRBO expression vector transiently expressed in leaves. Stable VLPs were formed, as confirmed by agarose gel electrophoresis, transmission electron microscopy and size exclusion chromatography. Interestingly, the morphology of the VLPs (15.8 ±1.3 nm icosahedral particles) differed from that of the native bacilliform particles indicating that the assembly of native virions is influenced by other viral proteins and/or the packaged viral genome. The smaller CiLV-C VLPs will also be useful for structure–function studies to compare with the 30-nm icosahedrons of other VLPs.

Graphical Abstract

* nsteinmetz@ucsd.edu .

Declaration of interests

Dr. Steinmetz is a co-founder of, has equity in, and has a financial interest with Mosaic ImmunoEngineering Inc. Dr. Steinmetz serves as Director, Board Member, and Acting Chief Scientific Officer, and paid consultant to Mosaic. The other authors declare no potential conflict of interest.

CRediT statements

Oscar A. Ortega-Rivera: Conceptualization, Methodology, Validation, Formal Analysis, Investigation, Writing – Original Draft, Visualization,

Veronique Beiss: Methodology, Validation, Formal Analysis, Investigation

Elizabeth O. Osota: Investigation

Soo Khim Chan: Investigation

Sweta Karan: Investigation, Visualization,

Nicole F. Steinmetz: Conceptualization, Validation, Resources, Data Curation, Writing – Review and Editing, Visualization, Supervision, Project Administration, Funding acquisition

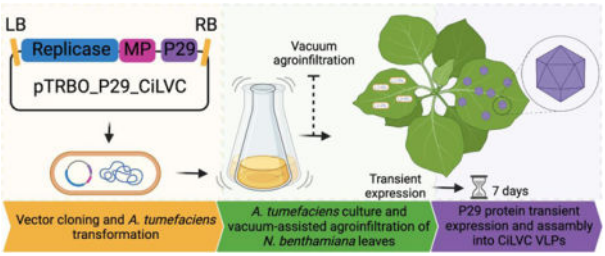

The production and testing of cytoplasmic type citrus leprosis virus-like particles (CiLV-C VLPs) began with the introduction of the *p29* gene encoding the CiLV-C capsid protein into the pTRBO vector to form pTRBO_P29_CiLVC, which was introduced into *Agrobacterium tumefaciens* strain GV3101 (left panel). Transient expression in *Nicotiana benthamiana* leaves was then facilitated by vacuum-assisted agroinfiltration (middle panel). After 7 days, the VLPs were extracted from detached leaves for testing. Abbreviations: LB = left border; RB = right border; replicase/MP = the RNA-dependent RNA polymerase and movement protein from tobacco mosaic virus; P29 = *p29* gene encoding the 29-kDa CiLV-C capsid protein.

Introduction

Plant viruses are widely used as platform technologies and nanoparticles that can be repurposed and engineered for diverse applications, including the investigation of viral assembly mechanisms [1], the development of nanocontainers for catalysts or drugs [2], precision farming [3, 4] as well as veterinary [5] and human health [6]. Plant viruses and their non-infectious counterparts, the virus-like particles (VLPs) are particularly promising as vaccine and immunotherapy platforms. For example, a COVID-19 vaccine candidate based on tobacco mosaic virus (TMV) was produced by Kentucky BioScience International, LLC [7]. Indeed, much research and many applications have focused on use of TMV, which is a 300 × 18 nm hollow nanotube in its native state but can also form spherical nanoparticles upon heat transformation [8]. Many different icosahedral plant viruses have been studied and engineered, many of which form 30-nm particles with T = 3 or pT = 3 symmetry. Examples include cowpea mosaic virus (CPMV) [9], cowpea chlorotic mottle virus (CCMV) [10], cucumber mosaic virus (CuMV) [11], red clover necrotic mottle virus (RCNMV) [4], and hibiscus chlorotic ringspot virus (HCRSV) [12]. Nanotechnology has taught us that the material properties and in vivo fate of nanoparticles are governed by their physiochemical characteristics, size and shape [13]. We therefore searched the International Committee on Taxonomy of Viruses (ICTV) database for plant viruses with different morphologies. This led us to cytoplasmic type citrus leprosis virus (CiLV-C), which forms bacilliform particles with dimensions of 60–70 nm × 110–120 nm.

CiLV-C causes citrus leprosis, a viral disease of citrus crops that is prevalent in South and Central America [14]. The disease is transmitted when plants are infested with mites (*Brevipalpus* spp.) and is caused by at least three viruses (CiLV-C being one of them), which establish non-systemic infections characterized by chlorotic lesions with necrotic ringspots on leaves, and chlorotic lesions and/or browning of fruits [14]. The disease results in fruit loss, stem dieback and in severe infestations can even kill citrus trees. The combined cost

of yield losses and chemical control measures for the prevention of mite infestations come to more than US$100 millions per year [15]. CiLV-C is the most widely distributed of the three viruses and is the type member of the genus *Cilevirus*, family Kitaviridae [16, 17]. Its bacilliform particles surround a positive-sense ssRNA genome in two segments, each featuring a 5′ cap and 3′ polyadenylate tail. The first segment (RNA1) contains two open reading frames (ORFs) encoding a multi-domain replication-associated protein and the capsid protein, p29 [14, 18, 19]. The second segment (RNA2) contains four ORFs encoding p15, which is required for the formation of vesicles in the ER [19], the p61 glycoprotein with roles in the remodeling of the ER and Golgi body [19, 20], the movement protein p32, and the integral membrane protein p24, which is also involved in viral replication and assembly in the ER and may function as a matrix protein [19].

To learn more about the assembly of CiLV-C, we transiently expressed the p29 capsid protein in *Nicotiana benthamiana* plants in an attempt to generate VLPs. Unlike native viruses, VLPs lack any genomic material and are therefore unable to replicate, but they are often structurally similar to the parental virus and still capable of interacting with target cells [21]. Therefore, CiLV-C VLPs would make a useful addition to the viral nanoparticle platforms currently being investigated. The availability of VLPs would also allow us to work on the development of more effective and less environmentally hazardous control measures to prevent citrus leprosis.

Methods

Expression and purification of CiLV-C VLPs

The wild-type CiLV-C p29 sequence (UniProt: Q1KZ58) was reverse translated and codon optimized for *N. benthamiana* using SnapGene. The cDNA was synthesized by Genscript Biotech and transferred from the source vector pUC57-mini_P29_CiLVC to the PacI-AvrII site of vector pTRBO (Addgene #80082) [22]. The insert was verified by colony PCR using primers TRBO-f (5′-GAT GAT TCG GAG GCT ACT GTC-3′) and P29-r 5′-CAG AAG GAC CAG GTT GAA GTT G-3′). The reaction was heated to 95 °C for 30 s followed by 30 cycles of 95 °C for 30 s, 60 °C for 30 s and 68 °C for 30 s, and a final elongation step at 68 °C for 5 min. The presence of the insert was confirmed by digestion with the restriction enzymes PacI and AvrII (New England Biolabs) followed by 1% (w/v) agarose gel electrophoresis. Further, the identity of the *p29* gene was validated by sequencing using Eurofins Genomics (Figure S1). Sequencing was performed on a PCR product obtained using pTRBO vector specific forward and reverse primers: TRBO FP 5’-GATGATTCGGAGGCTACTGTC-3’ and TRBO RP 5’-CTACCTCAAGTTGCAGGACCG-3’. Sequences data were analyzed by BlastN and BlastX analysis and CLUSTAL OMEGA sequence alignment.

Then *Agrobacterium tumefaciens* strain GV3101 (Gold Biotechnology) was transformed by electroporation and cultured at 28 °C in YEB medium (5 g/L beef extract, 1 g/L yeast extract, 5 g/L peptone, 5 g/L sucrose, 0.5 g/L $MgCl_2$) supplemented with 50 μg/ml kanamycin, 30 μg/ml gentamycin and 25 μg/ml rifampicin. Bacterial cultures were resuspended in infiltration buffer (10 mM MES pH 5.5, 10 mM $MgCl_2$, 2% (w/v) sucrose, 200 μM acetosyringone) and the OD_{600nm} was adjusted to 1. The suspension was incubated

for 4 h at room temperature before adding 0.01% (v/v) Silwet L-77 immediately prior to vacuum infiltration. Leaves of 6-week-old *N. benthamiana* plants were vacuum infiltrated as previously described [23] with an absolute pressure of 0.23 atm for 3 min before release. The infiltrated leaves were allowed to air dry under a fume hood for 1 h and the plants were then maintained at 24 °C and 60% humidity for 7 days with a 16-h photoperiod (10,000 lux). The leaves were harvested and stored at −80 °C.

The purification protocol was adapted from ref. [24]. VLPs were recovered from ~100 g of agroinfiltrated tissue by pulverization and homogenization in three volumes (300 mL) of cold 0.1 M sodium phosphate buffer (pH 7.0) containing 2% (w/v) polyvinylpolypyrrolidone (Sigma-Aldrich). The cell lysate was filtered through Miracloth to remove debris and centrifuged (12,000 × *g*, 20 min, 4 °C). The supernatant was supplemented with 0.2 M NaCl and 8% (w/v) PEG (MW 8000) and stirred overnight at 4 °C. The solution was centrifuged (14,000 × *g*, 15 min, 4 °C) and the pellet was redissolved in 50 ml 10 mM sodium phosphate buffer (pH 7.0) overnight. The next day, the solution was centrifuged (12,000 × *g*, 15 min, 4 °C) and the cleared supernatant was pelleted by ultracentrifugation (169,000 × *g*, 3 h, 4 °C). The pellet was resuspended in 2 ml 0.1 M sodium phosphate buffer (pH 7.0) overnight at 4 °C. Finally, the VLPs were purified by ultracentrifugation on a 30% sucrose cushion (133,000 × *g*, 3 h, 4 °C). The light scattering VLP band was collected, pelleted by ultracentrifugation (169,000 × *g*, 3 h, 4 °C), and the pellet was resuspended in 0.1 M sodium phosphate buffer (pH 7.0). The total protein concentration was determined using a BCA assay (Thermo Fisher Scientific).

Electrophoretic characterization of VLPs

The VLPs were characterized by denaturing sodium dodecyl sulfate polyacrylamide gel electrophoresis (SDS-PAGE) and agarose gel electrophoresis. For SDS-PAGE, we loaded 10-μg and 20-μg samples of total protein per lane on NuPAGE 4–12% gels and fractionated them for 37 min at 200 mV. The gels were stained with GelCode Blue Safe Protein Stain (Thermo Fisher Scientific). For agarose gel electrophoresis, 20-μg samples of total protein were loaded onto 1.2% (w/v) agarose gels and fractionated for 1 h at 80 mV. For nucleic acid identification the gel was stained with GelRed (Gold Biotechnology) and for protein identification the gel was stained with Coomassie Brilliant Blue. All gels were imaged using the ProteinSimple FluorChem R imaging system.

Transmission electron microscopy

Carbon-coated copper negative stain grids were glow-discharged for 30 s (easiGlow) before adding 10-μl samples of total protein, incubating for 2 min and blotting away excess liquid. The grids were washed twice in Milli-Q water before applying two lots of 10 μl 2% (w/v) uranyl acetate, leaving the stain for 30 s each time before blotting. The grids were air dried and analyzed on a JEOL JEM-1400 series 120kV Transmission Electron Microscope. The size of the CiLV-C VLPs was determined analyzing three images at different magnifications (60,000×, 80,000× and 100,000×) and measuring the diameter of 100 particles from five random fields (20 particles/field) in each image. The diameter of the 300 particles in total was presented as a frequency–size distribution histogram and the polydispersity index (PDI) was calculated as follows:

$$PDI = (\text{standard deviation / mean diameter size})^2$$

Size exclusion chromatography

CiLV-C VLPs were analyzed by size exclusion chromatography (SEC) using an AKTA Pure system fitted with a Superose 6 Increase 10/300 GL column (GE Healthcare). Samples (500 μg total protein) were analyzed at a flow rate of 0.5 ml/min using 0.1 M sodium phosphate buffer (pH 7.0).

Results and discussion

Cloning and expression of the CiLV-C p29 gene

The codon-optimized CiLV-C p29 sequence was synthesized by GenScript Biotech and provided in vector pUC57-mini_P29_CiLVC. We transferred the *p29* ORF to the pTRBO vector, which contains the TMV replicase and movement protein genes [22] and is widely used for the overexpression of recombinant proteins in plants (Figure 1a). The recombinant vector pTRBO_P29_CiLVC was introduced into *A. tumefaciens* strain GV3101 by electroporation, and the presence of the insert was confirmed by colony PCR (Figure 1b) and a diagnostic restriction assay, which yielded a product of ~813 bp in addition to the >10-kb linearized pTRBO backbone (Figure 1c). Finally, sequencing confirmed the identity of the *p29* gene (Figure S1).

The leaves of 6-week-old *N. benthamiana* plants were vacuum infiltrated with the suspension of *A. tumefaciens* and left to express the p29 protein for 7 days. VLPs were then recovered from leaf extracts by ultracentrifugation over a 30% sucrose cushion (Figure 2a–c). Agarose gel electrophoresis showed that extracts before and after ultracentrifugation contained comigrating nucleic acid and protein bands (Figure 2d). VLPs lack genomic RNA, but often package random host RNA molecules based on nonspecific electrostatic interactions with the nucleic acid backbone [25], given the absence of a common packaging motif. We will investigate the nature of these captured RNA molecules in future work. SDS-PAGE under denaturing conditions confirmed the presence of the 29-kDa capsid protein in the crude extract before ultracentrifugation, and in the VLP band, but not in the pellet (Figure 2e).

Size and morphology of the CiLV-C VLPs

TEM analysis of the VLP band as well as pellet was performed confirming the presence of VLPs only in the light scattering band, denoted as the VLP band (Figure S2). Once we confirmed the presence of VLPs in the light scattering band, the samples were further analyzed by SEC which revealed one major peak at ~ 15 mL (Figure 3a). Fractions were analyzed by SDS-PAGE revealing a 29-kDa protein the in major peak fraction (Figure 3b). Finally, TEM imaging of the major peak fraction also confirmed the presence of icosahedral particles (Figure 3c). The original morphological description of CiLV-C referred to short bacilliform particles (60–70 nm × 110–120 nm) in the cisternae of the ER, as well as electron-dense viroplasms distributed in the cytoplasm [26]. However, the analysis of TEM

images revealed an icosahedral morphology with T = 1 symmetry (Figure 3c) and the VLPs were also smaller in size than the native particles (15.8 ±1.3 nm) with a PDI of 0.006 (Figure S3).

Our goal was to produce bacilliform VLPs larger than the typical 30-nm icosahedrons formed by other plant viruses. Although the CiLV-C VLPs did not assemble into the anticipated bacilliform particles, the icosahedral particles with T = 1 symmetry were smaller than usual (~15 nm) and offer an opportunity to test for size-specific behavior during cell uptake and in vivo trafficking. VLPs that self-assemble from capsid proteins expressed in microbes, animal cells, plant cells or cell-free systems often resemble the structure of the parent virus, but this is not always the case. For example, in contrast to most members of the *Alfamovirus* genus, many strains of alfalfa mosaic virus (AlMV) are composed of bacilliform particles, but expressing the coat protein in *Escherichia coli* produces icosahedral particles with T = 1 symmetry similar to those we observed for CiLV-C [27, 28]. This is likely to reflect the absence of viral genomic RNA, which normally coordinates the assembly of coat protein subunits. Indeed. AlMV can form particles with various morphologies, including bacilliform, icosahedral and long tubular structures resembling the cross-section of the icosahedral capsid (with or without icosahedral end caps) depending on the presence/absence of nucleic acids [29] and the specific type: heterologous virus genome, calf thymus DNA, yeast total RNA, or poly(A) RNA [30, 31]. These morphologies can also be replicated by limited trypsin digestion [32] and by coat protein mutants that influence the formation of coat protein dimers (as the basic unit of capsid assembly) and the choice between the formation of pentamers or hexamers [28, 33]. Furthermore, to restore the bacilliform of CiLV-C, co-expression of additional structural proteins may be necessary. The integral membrane protein p24, has been implicated to play a role as a matrix protein [19], and thus may be required for assembly of the bacilliform. We also note that it may also be possible that bacilliform particles might be present but are less stable or are present at too low titers and possibly do not elute in the expected purification fractions.

Conclusion

We expressed the CiLV-C p29 capsid protein in *N. benthamiana* and confirmed that it self-assembles into stable VLPs, albeit differing in size and morphology from the native CiLV-C particles. Such differences are often observed when some of the components required to assemble native particles are missing (in this case, the most likely candidates are the native RNA1 and RNA2, but potentially also one or more of the five additional CiLV-C proteins). The production of CiLV-C VLPs provides insight into the assembly mechanism and may facilitate the development of more effective countermeasures against citrus leprosis based on the direct inhibition of the viral replication cycle. CiLV-C VLPs could also be developed as delivery platforms for drugs, vaccines, and imaging reagents.

Supplementary Material

Refer to Web version on PubMed Central for supplementary material.

Acknowledgments

This work was supported in part by a grant from the National Institute of Health (U01 CA218292, R21 AI161306, R01 CA224605 to N.F.S.) and the National Science Foundation through the UC San Diego Materials Research Science and Engineering Center (DMR-2011924 to N.F.S.). O.A.O.-R. acknowledges the UC MEXUS-CONACYT Postdoctoral Fellowship 2019–2020 number FE-19-58. E.O.O. was supported by the NIH 2T32 CA153915-06A1 institutional training grant through the Cancer Research in Nanotechnology San Diego Fellowship.

References:

[1]. Twarock R, Stockley PG, RNA-Mediated Virus Assembly: Mechanisms and Consequences for Viral Evolution and Therapy, Annu Rev Biophys 48 (2019) 495–514. [PubMed: 30951648]

[2]. Steinmetz NF, Lim S, Sainsbury F, Protein cages and virus-like particles: from fundamental insight to biomimetic therapeutics, Biomater Sci 8(10) (2020) 2771–2777. [PubMed: 32352101]

[3]. Chariou PL, Dogan AB, Welsh AG, Saidel GM, Baskaran H, Steinmetz NF, Soil mobility of synthetic and virus-based model nanopesticides, Nat Nanotechnol 14(7) (2019) 712–718. [PubMed: 31110265]

[4]. Cao J, Guenther RH, Sit TL, Lommel SA, Opperman CH, Willoughby JA, Development of abamectin loaded plant virus nanoparticles for efficacious plant parasitic nematode control, ACS Appl Mater Interfaces 7(18) (2015) 9546–53. [PubMed: 25906360]

[5]. Hoopes PJ, Wagner RJ, Duval K, Kang K, Gladstone DJ, Moodie KL, Crary-Burney M, Ariaspulido H, Veliz FA, Steinmetz NF, Fiering SN, Treatment of Canine Oral Melanoma with Nanotechnology-Based Immunotherapy and Radiation, Mol Pharm 15(9) (2018) 3717–3722. [PubMed: 29613803]

[6]. Chung YH, Church D, Koellhoffer EC, Osota E, Shukla S, Rybicki EP, Pokorski JK, Steinmetz NF, Integrating plant molecular farming and materials research for next-generation vaccines, Nat Rev Mater 7(5) (2022) 372–388. [PubMed: 34900343]

[7]. Royal JM, Simpson CA, McCormick AA, Phillips A, Hume S, Morton J, Shepherd J, Oh Y, Swope K, DeBeauchamp JL, Webby RJ, Cross RW, Borisevich V, Geisbert TW, Demarco JK, Bratcher B, Haydon H, Pogue GP, Development of a SARS-CoV-2 Vaccine Candidate Using Plant-Based Manufacturing and a Tobacco Mosaic Virus-like Nano-Particle, Vaccines (Basel) 9(11) (2021).

[8]. Atabekov J, Nikitin N, Arkhipenko M, Chirkov S, Karpova O, Thermal transition of native tobacco mosaic virus and RNA-free viral proteins into spherical nanoparticles, J Gen Virol 92(Pt 2) (2011) 453–6. [PubMed: 20980527]

[9]. Lizotte PH, Wen AM, Sheen MR, Fields J, Rojanasopondist P, Steinmetz NF, Fiering S, In situ vaccination with cowpea mosaic virus nanoparticles suppresses metastatic cancer, Nat Nanotechnol 11(3) (2016) 295–303. [PubMed: 26689376]

[10]. Brasch M, Putri RM, de Ruiter MV, Luque D, Koay MS, Caston JR, Cornelissen JJ, Assembling Enzymatic Cascade Pathways inside Virus-Based Nanocages Using Dual-Tasking Nucleic Acid Tags, J Am Chem Soc 139(4) (2017) 1512–1519. [PubMed: 28055188]

[11]. Nuzzaci M, Piazzolla G, Vitti A, Lapelosa M, Tortorella C, Stella I, Natilla A, Antonaci S, Piazzolla P, Cucumber mosaic virus as a presentation system for a double hepatitis C virus-derived epitope, Arch Virol 152(5) (2007) 915–28. [PubMed: 17238010]

[12]. Ren Y, Wong SM, Lim LY, Folic acid-conjugated protein cages of a plant virus: a novel delivery platform for doxorubicin, Bioconjug Chem 18(3) (2007) 836–43. [PubMed: 17407258]

[13]. Toy R, Peiris PM, Ghaghada KB, Karathanasis E, Shaping cancer nanomedicine: the effect of particle shape on the in vivo journey of nanoparticles, Nanomedicine (Lond) 9(1) (2014) 121–34. [PubMed: 24354814]

[14]. Locali-Fabris EC, Freitas-Astua J, Souza AA, Takita MA, Astua-Monge G, Antonioli-Luizon R, Rodrigues V, Targon M, Machado MA, Complete nucleotide sequence, genomic organization and phylogenetic analysis of Citrus leprosis virus cytoplasmic type, J Gen Virol 87(Pt 9) (2006) 2721–2729. [PubMed: 16894213]

[15]. Rodrigues JCV, Relações patógeno-vetor-planta no sistema leprose dos citros, Centro de Energia Nuclear na Agricultura, Universidade de São Paulo, 2000.

[16]. Freitas-Astua J, Ramos-Gonzalez PL, Arena GD, Tassi AD, Kitajima EW, Brevipalpus-transmitted viruses: parallelism beyond a common vector or convergent evolution of distantly related pathogens?, Curr Opin Virol 33 (2018) 66–73. [PubMed: 30081359]

[17]. Chabi-Jesus C, Ramos-Gonzalez PL, Postclam-Barro M, Fontenele RS, Harakava R, Bassanezi RB, Moreira AS, Kitajima EW, Varsani A, Freitas-Astua J, Molecular Epidemiology of Citrus Leprosis Virus C: A New Viral Lineage and Phylodynamic of the Main Viral Subpopulations in the Americas, Front Microbiol 12 (2021) 641252. [PubMed: 33995302]

[18]. Pascon RC, Kitajima JP, Breton MC, Assumpcao L, Greggio C, Zanca AS, Okura VK, Alegria MC, Camargo ME, Silva GG, Cardozo JC, Vallim MA, Franco SF, Silva VH, Jordao H Jr., Oliveira F, Giachetto PF, Ferrari F, Aguilar-Vildoso CI, Franchiscini FJ, Silva JM, Arruda P, Ferro JA, Reinach F, da Silva AC, The complete nucleotide sequence and genomic organization of Citrus Leprosis associated Virus, Cytoplasmatic type (CiLV-C), Virus Genes 32(3) (2006) 289–98. [PubMed: 16732481]

[19]. Leastro MO, Kitajima EW, Silva MS, Resende RO, Freitas-Astua J, Dissecting the Subcellular Localization, Intracellular Trafficking, Interactions, Membrane Association, and Topology of Citrus Leprosis Virus C Proteins, Front Plant Sci 9 (2018) 1299. [PubMed: 30254655]

[20]. Kuchibhatla DB, Sherman WA, Chung BY, Cook S, Schneider G, Eisenhaber B, Karlin DG, Powerful sequence similarity search methods and in-depth manual analyses can identify remote homologs in many apparently “orphan” viral proteins, J Virol 88(1) (2014) 10–20. [PubMed: 24155369]

[21]. Zeltins A, Construction and characterization of virus-like particles: a review, Mol Biotechnol 53(1) (2013) 92–107. [PubMed: 23001867]

[22]. Lindbo JA, TRBO: a high-efficiency tobacco mosaic virus RNA-based overexpression vector, Plant Physiol 145(4) (2007) 1232–40. [PubMed: 17720752]

[23]. Plesha MA, Huang TK, Dandekar AM, Falk BW, McDonald KA, Optimization of the bioprocessing conditions for scale-up of transient production of a heterologous protein in plants using a chemically inducible viral amplicon expression system, Biotechnol Prog 25(3) (2009) 722–34. [PubMed: 19504593]

[24]. Murray AA, Sheen MR, Veliz FA, Fiering SN, Steinmetz NF, In Situ Vaccination of Tumors Using Plant Viral Nanoparticles, Methods Mol Biol 2000 (2019) 111–124. [PubMed: 31148013]

[25]. Mohsen MO, Gomes AC, Vogel M, Bachmann MF, Interaction of Viral Capsid-Derived Virus-Like Particles (VLPs) with the Innate Immune System, Vaccines (Basel) 6(3) (2018).

[26]. Kitajima EW, Muller GW, Costa AS, Yuki W, Short, rod-like particles associated with Citrus leprosis, Virology 50(1) (1972) 254–8. [PubMed: 4117125]

[27]. Yusibov V, Kumar A, North A, Johnson JE, Loesch-Fries LS, Purification, characterization, assembly and crystallization of assembled alfalfa mosaic virus coat protein expressed in Escherichia coli, J Gen Virol 77 (Pt 4) (1996) 567–73. [PubMed: 8627243]

[28]. Choi J, Loesch-Fries LS, Effect of C-terminal mutations of alfalfa mosaic virus coat protein on dimer formation and assembly in vitro, Virology 260(1) (1999) 182–9. [PubMed: 10405370]

[29]. Fukuyama K, Abdel-Meguid SS, Johnson JE, Rossmann MG, Structure of a T = 1 aggregate of alfalfa mosaic virus coat protein seen at 4.5 A resolution, J Mol Biol 167(4) (1983) 873–90. [PubMed: 6876169]

[30]. Hull R, Studies on alfalfa mosaic virus. 3. Reversible dissociation and reconstitution studies, Virology 40(1) (1970) 34–47. [PubMed: 5411192]

[31]. Driedonks RA, Krijgsman PC, Mellema JE, Alfalfa mosaic virus protein polymerization, J Mol Biol 113(1) (1977) 123–40. [PubMed: 18611]

[32]. Bol JF, Kraal B, Brederode FT, Limited proteolysis of alfalfa mosaic virus: influence on the structural and biological function of the coat protein, Virology 58(1) (1974) 101–10. [PubMed: 4362543]

[33]. Kumar A, Reddy VS, Yusibov V, Chipman PR, Hata Y, Fita I, Fukuyama K, Rossmann MG, Loesch-Fries LS, Baker TS, Johnson JE, The structure of alfalfa mosaic virus capsid protein assembled as a T=1 icosahedral particle at 4.0-A resolution, J Virol 71(10) (1997) 7911–6. [PubMed: 9311881]

Research highlights

- Virus like particles (VLPs) of Cytoplasmic type citrus leprosis virus (CiLV-C) were produced through transient expression in plants.
- Native CiLV-C forms bacilliform particles (60–70 nm × 110–120 nm).
- The CiLV-C capsid protein (p29) gene was transferred to the pTRBO expression vector and introduced into *Agrobacterium tumefaciens* strain GV3101 followed by the vacuum-assisted agroinfiltration of *N. benthamiana* leaves.
- Stable VLPs were formed and interstingly the morphology of the VLPs (15.8 ±1.3 nm icosahedral particles) differed from that of the native bacilliform particles.
- The smaller CiLV-C VLPs will also be useful for structure–function studies to compare with the 30-nm icosahedrons of other VLPs.
- The production of CiLV-C VLPs provides insight into the assembly mechanism of the virus, which may guide the development of more effective countermeasures against citrus leprosis.

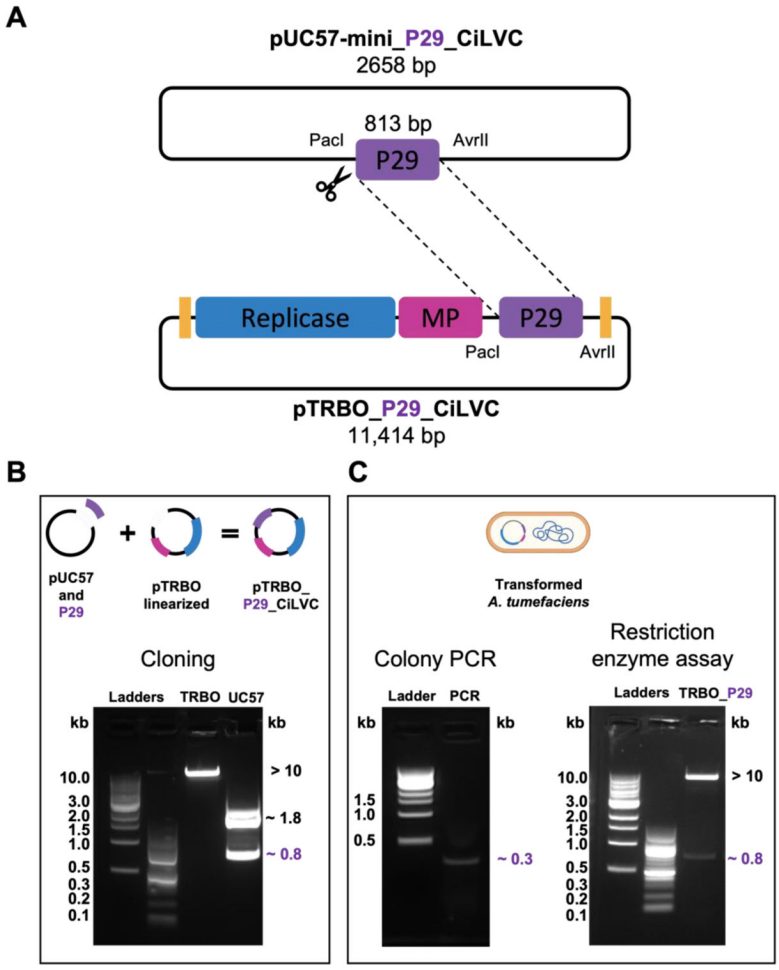

Figure 1.

Cloning of the CiLV-C *p29* gene in a plant expression vector. (A) The *p29* gene was transferred from its source vector pUC57-mini_P29_CiLVC to the pTRBO (tobacco mosaic virus RNA-based overexpression) vector using the restriction enzymes PacI and AvrII, yielding the final vector pTRBO_P29_CiLVC. (B) Digestion of pUC57-mini_P29_CiLVC with PacI and AvrII, releasing the *p29* gene as an 813-bp fragment. The same enzymes were used to linearize pTRBO to allow unidirectional ligation. (C) Following the electroporation of *A. tumefaciens* strain GV3101 with pTRBO_P29_CiLVC, the presence of the insert was confirmed by colony PCR to yield a 307-bp product, and by a diagnostic restriction digest to release the entire 813-bp insert along with the >10-kb linearized pTRBO backbone. Lastly, sequencing confirmed the identity of the *p29* gene (Figure S1).

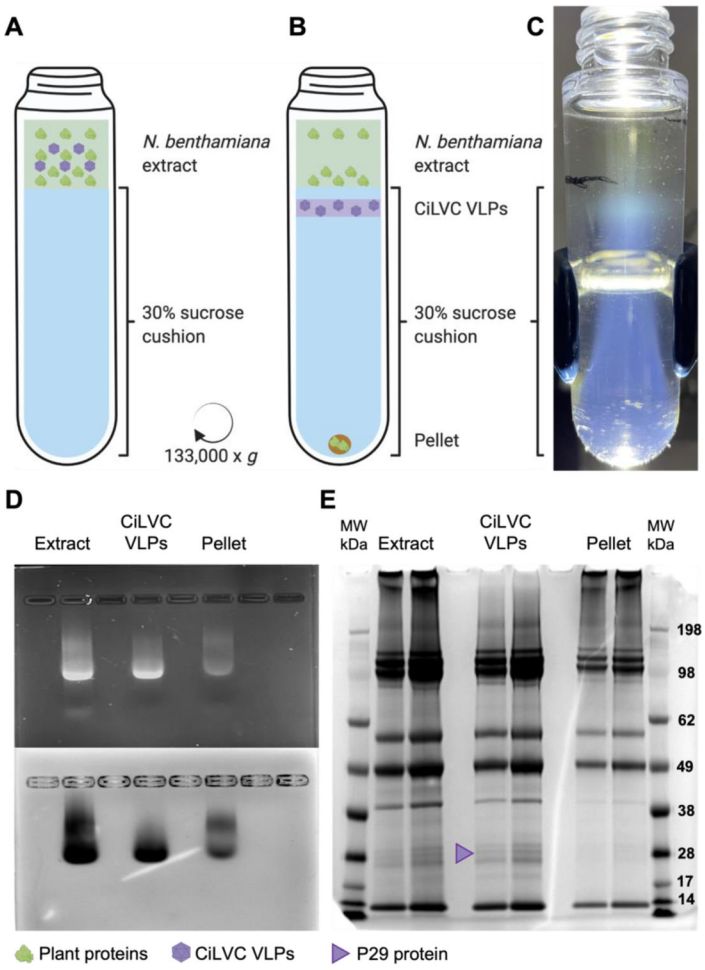

Figure 2.

Purification and analysis of CiLV-C VLPs. (A-C) Schematic illustration of the sucrose cushion ultracentrifugation step. (A) The *N. benthamiana* leaf extract was loaded onto the 30% sucrose cushion. (B) After ultracentrifugation, the CiLV-C VLPs formed a band at the top of the sucrose cushion and most plant proteins either remained in the aqueous zone or formed a pellet. (C) Image of a tube after ultracentrifugation showing the CiLV-C VLP band. (D) Analysis of 20 μg of total protein from the crude extract (left), the VLP band (middle) and the pellet (right) by 1.2% agarose gel electrophoresis. The top image shows nucleic acid staining (GelRed) and the bottom image shown protein staining (Coomassie Brilliant Blue) confirming the comigration of protein and nucleic acid in intact VLPs. (E) Denaturing SDS-PAGE in 4–12% polyacrylamide gels of 10 and 20 μg of total protein from the crude extract (left), the VLP band (middle) and the pellet (right), indicating the presence of p29 in the crude extract and VLPs but not the pellet.

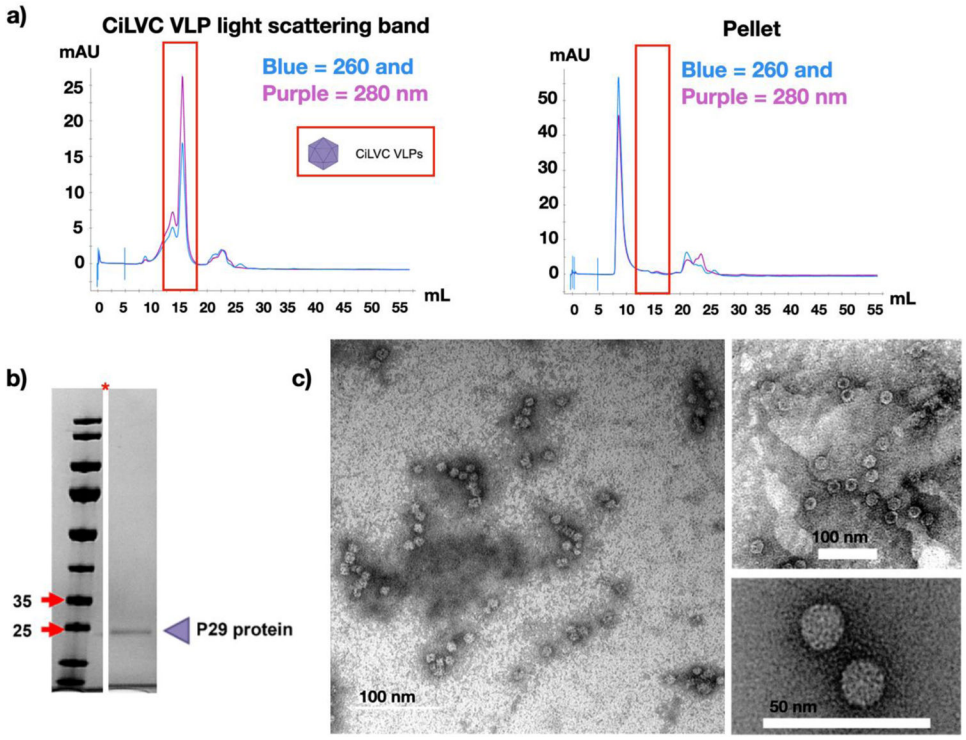

Figure 3.

Purification of CiLV-C VLPs by size exclusion chromatography (SEC) and characterization of the fractions. (A) SEC revealed one major peak at ~ 15 mL for the light scattering band (CiLV-C VLPs band in Figure 2b) – larger, possibly aggregates were observed when the pellet fraction was subjected to SEC analysis. (B) SDS-PAGE analysis in 4–12% polyacrylamide gels under denaturing conditions reveals the presence of the p29 protein in the major peak fraction. (C) TEM images of the major peak fraction showing pure CiLV-C VLPs (49,000×, scale bar = 100 nm; and 128,000×, scale bar = 50 nm).